Ambiguity-Free Doppler Centroid Estimation Technique for Airborne SAR Using the Radon Transform

Young-Kyun Kong, Byung-Lae Cho, and Young-Soo Kim, *Member, IEEE*

***Abstract*—In synthetic aperture radar (SAR) signal processing, the Doppler centroid estimation technique, called the "clutter-lock," is important because it is related to the signal-to-noise ratio, geometric distortion, and radiometric error of the final SAR image. Conventional algorithms have either ambiguity problems or somewhat high computational load. Using the fact that the Doppler centroid and the squint angle are directly related, we propose an ambiguity-free Doppler centroid estimation technique using Radon transform, named geometry-based Doppler estimator. The proposed algorithm is computationally efficient and shows good performance of estimating the absolute Doppler centroid.**

***Index Terms*—Clutter-lock, Doppler ambiguity resolver (DAR), Doppler ambiguity resolver, Doppler centroid estimation, synthetic aperture radar (SAR).**

I. Introduction

SYNTHETIC aperture radar (SAR) is a radar system which has the purpose of obtaining two-dimensional images of the target area. It flies in a straight nominal path and periodically receives a back-scattered signal from the target area. High azimuth resolution is obtained by coherently processing the Doppler histories of the return signal. This procedure is called azimuth compression, and here several important parameters such as the Doppler centroid and Doppler frequency rate are required. Inaccurate Doppler centroid results in low signal-to-noise ratio (SNR), geometric distortion and radiometric error of the SAR image, and Doppler frequency rate has an effect on the focus of the SAR image. Estimation of Doppler centroid and Doppler frequency rate are called clutter-lock and autofocus, respectively. Several clutter-lock techniques have been proposed so far. They are energy balancing (ΔE), correlation Doppler estimator (CDE), sign Doppler estimator (SDE) [1], and maximum-likelihood estimation (MLE) [2]. The performances of these algorithms are compared in [4] and [5]. One of the major concerns in clutter-lock is how to deal with Doppler ambiguity. CDE, SDE, and ΔE are the baseband algorithms which do not resolve the Doppler ambiguity and do not work well if partially exposed strong targets exist in the raw data. Such raw data can be obtained from high-contrast scenes such as urban and coastal areas. To resolve the Doppler ambiguity, some Doppler ambiguity resolvers (DARs) are proposed, such as multilook cross-correlation (MLCC) and multilook beat frequency (MLBF) [3], the range look correlation technique [6], [8], and the wavelength diversity algorithm (WDA) [7]. The range look correlation technique estimates the Doppler ambiguity only, and as this lacks sensitivity, its reliability is not guaranteed for all the cases [3]. WDA and MLCC-MLBF can estimate the Doppler centroid and can resolve the Doppler ambiguity. WDA works best in the low-contrast scenes. MLCC-MLBF seems to be the best algorithm so far that estimates both the Doppler centroid and the Doppler ambiguity. However, its computational load is somewhat high, because it requires fast Fourier and inverse fast Fourier transforms to generate multilook range-compressed data. Nowadays, as computer technology is getting advanced in both hardware and software, the computational load of an algorithm can be considered less important, from a certain point of view. The proposed algorithm in this paper has completely different approach than the MLCC-MLBF to estimate both the Doppler centroid and the Doppler ambiguity number. The proposed algorithm utilizes the range walk response of targets induced by the squinted beam and does not use the signal power spectra. It requires no Fourier transform and is performed in a down-sampled range-compressed domain. Therefore, this algorithm does not have an ambiguity problem. Although the proposed algorithm is not always faster than CDE or SDE, taking its capability of resolving ambiguity into consideration, the propose algorithm is computationally efficient.

II. Conventional Clutter-Lock Algorithms and the Shape of Target Responses

Consider the case of an airborne stripmap mode SAR as shown in Fig. 1(a). s is slow time, V_{st} is the platform forward velocity, θ_s is squint angle, λ_c is the wavelength at carrier frequency, and f_{DC} is the Doppler centroid. In this condition, f_{DC} is given as follows:

$$f_{\mathrm{DC}} = \frac{2V_{st}}{\lambda_c}\sin\theta_s \tag{1}$$

and the squint angle is defined as

$$\sin\theta_s = \frac{\sqrt{R_0^2(r)-h^2}}{R_0(r)}\sin\theta_d \tag{2}$$

Manuscript received July 24, 2004; revised December 22, 2004. This work was supported by the Ministry of Information and Communication, Korea, under the Information Technology Research Center support program supervised by the Institute of Information Technology Assessment.

The authors are with the Division of Electrical and Computer Engineering, Pohang University of Science and Technology, Gyungbuk, Korea (e-mail: unknown@postech.ac.kr; chobl@postech.ac.kr; ysk@postech.ac.kr).

Digital Object Identifier 10.1109/TGRS.2005.843955

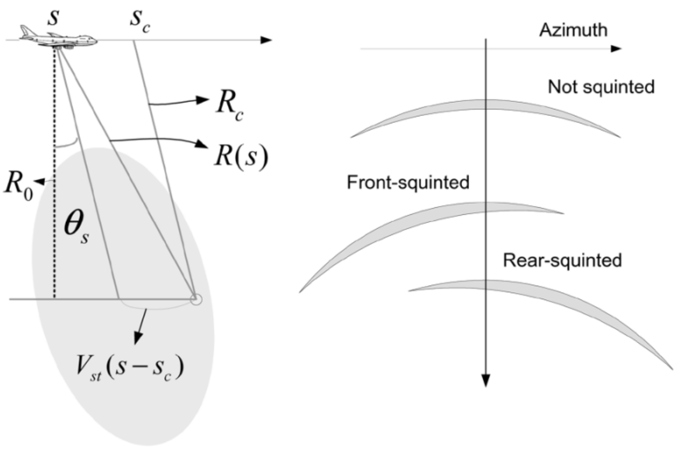

Fig. 1. Examples of SAR geometry and the target responses. (a) SAR geometry. (b) The target responses in different cases of squint angle.

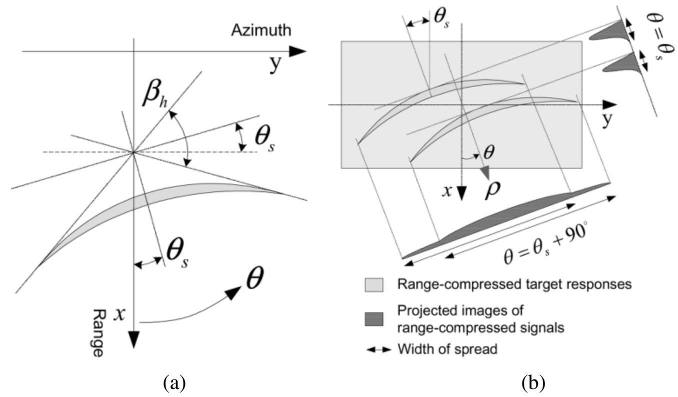

Fig. 2. (a) Angle information contained in the response of a point target. (b) Projection of range-compressed image along the lines with the angles $\theta = \theta_s$ and $\theta = \theta_s + 90^\circ$ with respect to the positive x axis.

where θ_d is the drift angle, $R_0(r)$ is the range at the closest approach, and r is the range index.

The purpose of the clutter-lock algorithm is to estimate the Doppler centroid, which is an important parameter that has effects on SNR, geometric distortion, and radiometric error of the final SAR image. The ΔE algorithm is performed in the Doppler frequency domain obtained by a Fourier transform, which requires a high computational load. To reduce the computational load, two time-domain algorithms, CDE and SDE, were introduced. CDE and SDE used the fact that if the power spectrum is shifted, the phase of corresponding autocorrelation function changes. Although the performances of ΔE, CDE, and SDE are different, these algorithms are equivalent from the viewpoint that these are based on the correlation of a signal power spectrum with a particular weighting function [4], [5]. Because the spectrum of the sampled signal has periodicity, it is impossible to find the ambiguity number without any additional techniques. Now, let us investigate the target response in the range-compressed domain. The response of a target in the range-compressed domain is approximately quadratic. Fig. 1(b) shows the examples of target responses in three different cases of squint angles for the SAR geometry shown in Fig. 1(a). As seen from Fig. 1(b), the shape of the target response depends on the squint angle, even if the relative positions of the target and the SAR platform are the same. But, as all the responses of targets in the scene contain the same angle information (θ_s, β_h), it is not difficult to extract this information from the range-compressed image. In conventional clutter-lock algorithms, the shape of the target response in the range-compressed image was not taken into consideration for estimating the Doppler centroid. Among the DAR algorithms, the range look correlation technique uses two azimuth looks to measure misregistration in the range direction [6]. It uses the geometry of the range-compressed data. But, as mentioned in the previous section, it estimates only the ambiguity number. The proposed algorithm uses angle information contained in the response of targets and is named geometry-based Doppler estimator (GDE), as it estimates the absolute Doppler centroid (the ambiguous Doppler centroid and the Doppler ambiguity number) based on the geometry of the target responses.

III. New Ambiguity-Free Clutter-Lock Algorithm

A. Algorithm Description

As described in Section II, the shape of a target response contains the information about the squint angle and beamwidth. If this information is extracted successfully, the Doppler centroid can be calculated using (1). Fig. 2(a) shows the angle information contained in the range-compressed target response. One is the antenna beamwidth (β_h), which is a known value, and the other is squint angle (θ_s) which is the average inclination of the target response. Here, to locate the range of angles in which the target response exists, we propose to use the Radon transform. The Radon transform is normally used to detect straight lines in an image and is defined as the integral along the straight line defined by its distance from the origin and the angle with respect to the positive x axis. A line in $g(x,y)$ is mapped into a point in $\hat{g}(\rho,\theta)$ by the following equation:

$$\hat{g}(\rho,\theta) = \int_{-\infty}^{\infty}\int_{-\infty}^{\infty} g(x,y)\delta(\rho - x\cos\theta - y\sin\theta)dxdy. \quad (3)$$

The flowchart of GDE is shown in Fig. 3. As the Doppler centroid f_{DC} varies with range, as seen from (2), segmentation of the range-compressed data in the range direction may be performed before applying GDE because GDE assumes that the squint angle is invariant with range. Let δx be the range sampling interval and δy be the azimuth sampling interval. In case of an airborne SAR, in general, δx is several times (> 10) larger than δy; therefore, $R = \lfloor \delta x/\delta y + 0.5 \rfloor > 10$, where $\lfloor a \rfloor$ takes the smallest integer not greater than a. For example, if the sampling frequency $f_s = 150$ MHz, PRF $= 2$ kHz, and $V_{st} = 100$ m/s, then R equals to 20. To improve computational efficiency, down-sampling the raw data by factor R in azimuth direction is required. Next, as mentioned above, the range compression of the raw data is performed. Further down-sampling of the range-compressed image by a factor D can be performed as the cases may require. Then, take the magnitude of samples and perform the Radon transform within the angles of interest. When performing the Radon transform, the maximum angular step size $\Delta\theta$ must be less than $\beta_h/3$. If no prior information about the squint angle is available, perform the Radon transform in wide range of angles with coarse step size, e.g., from -30° to 30° with the step size of 2°. The transformed

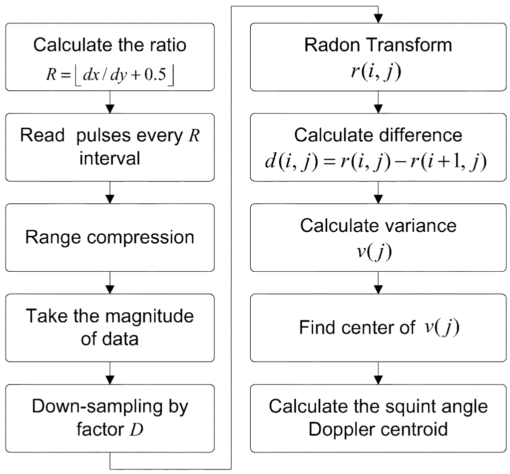

Fig. 3. Flowchart of GDE.

image is $r(i,j) = \hat{g}(\rho_0 + i\Delta\rho, \theta_0 + j\Delta\theta)$, $0 < i < N-1$, $0 < j < M-1$, where i, j are the indexes of distance and angle, $\Delta\rho$ and $\Delta\theta$ are the step size in distance (ρ) and angle (θ) directions, and θ_0 and ρ_0 are the start angle and the start distance of the Radon transform, respectively. The result of the Radon transform is a collection of curves concentrated in the angles corresponding to the direction of the antenna beam. Therefore, it is required to locate the range of angles in which the transformed lines are concentrated. The key here is that the transformed images in that region are "rough" in distance (ρ) direction. This can be easily understood if Fig. 2(b) is referred. The projected image of a point target response is concentrated in smaller region if the projection angle θ is closer to θ_s, as seen from the case of $\theta = \theta_s$ in Fig. 2(b). In contrast, if the projection angle θ is far from θ_s, the projected image of a target response is spread over a wide region, as seen from the case of $\theta = \theta_s + 90^\circ$ in Fig. 2(b). The rougher the signal, the greater the variance of difference signals. In other words, the transformed images are less dispersed in the distance direction when the angle is equal to the true squint angle, and at this angle the differences have a higher variance. Therefore, the variance of the difference signal is used here as the measure of roughness as follows:

$$v(j) = \frac{1}{N-1}\sum_{i=0}^{N-2} d^2(i,j) - \left\{\frac{1}{N-1}\sum_{i=0}^{N-2} d(i,j)\right\}^2. \quad (4)$$

Detecting the peak of $v(j)$ is not a good way of finding squint angle because the peak of $v(j)$ may not always be located at the center of the beam. Furthermore, energy-balancing techniques may not produce a satisfactory result because $v(j)$ does not have periodicity. To solve this problem, we used the radial basis function network (RBFN) with one hidden layer with one neuron [9]. The RBFN was trained with normalized signal $\hat{v}(j) = \{v(j) - v_{\min}\}/\{v_{\max} - v_{\min}\}$, where $v_{\max}$ and $v_{\min}$ are the maximum and minimum values of $v(j)$, respectively. The initial center of the Gaussian basis function was selected as the peak position, and the initial width of the basis function was calculated from the antenna beamwidth. Once the function approximation is obtained, the center of the basis function represents the estimate of of squint angle.

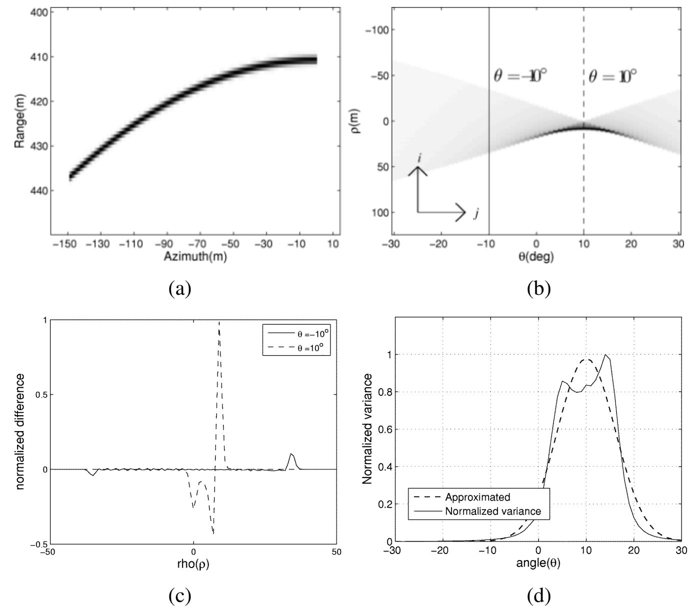

Fig. 4. Simulation results of the GDE with one point target. (a) The range-compressed image. (b) The Radon-transformed image. The center of the Radon transform was selected at the center of range-compressed image. (c) Plot of difference signals at the angles of -10° and 10°. (d) Plot of variances of difference signals at each angle.

B. Implementations of the Radon Transform

Our SAR processor is written in C++ and runs on the Win32 platform. To implement the Radon transform in our SAR processor, we referred the "radon" function in MATLAB 6.5 (RT algorithm 1) and the algorithm (RT algorithm 2) described in the Section II of [10]. RT Algorithm 1 uses a virtual computation grid to obtain the effect of oversampling of factor 2 and performs linear interpolation to enhance the accuracy of computation. On the other hand, no accuracy enhancement technique is adopted in RT algorithm 2. We implemented these two algorithms in C++ and used Intel's integrated performance primitives 4.0 to make those faster.

IV. Simulations

To verify the performance of GDE, we performed simulations of the cases of one point scatterer and multiple point scatterers. All simulations were performed on the computer with Intel Pentium IV 2.8 GHz, 2 GB of dual-channel DDR400 RAM.

A. Case of One Point Scatterer

First, we performed simulation with a one point scatterer located at the range of 410 m. Simulation parameters are $\beta_h = 10^\circ$, $\theta_s = 10^\circ$, PRF $= 4$ kHz, $f_s = 150$ MHz, and $V_{st} = 100$ m/s. Because of the nonzero squint angle, the range-compressed target response and the Radon-transformed image are asymmetrical as shown in Fig. 4(a) and (b). Fig. 4(c) shows the difference signals at the angles of -10° and 10°. As expected, the roughness of the difference signal at $\theta = 10^\circ$, which is the squint angle, is greater than the roughness at $\theta = -10^\circ$. Finally, the squint angle is estimated to be $\theta_s = 10^\circ$ using RBFN function approximation of variances of difference signal.

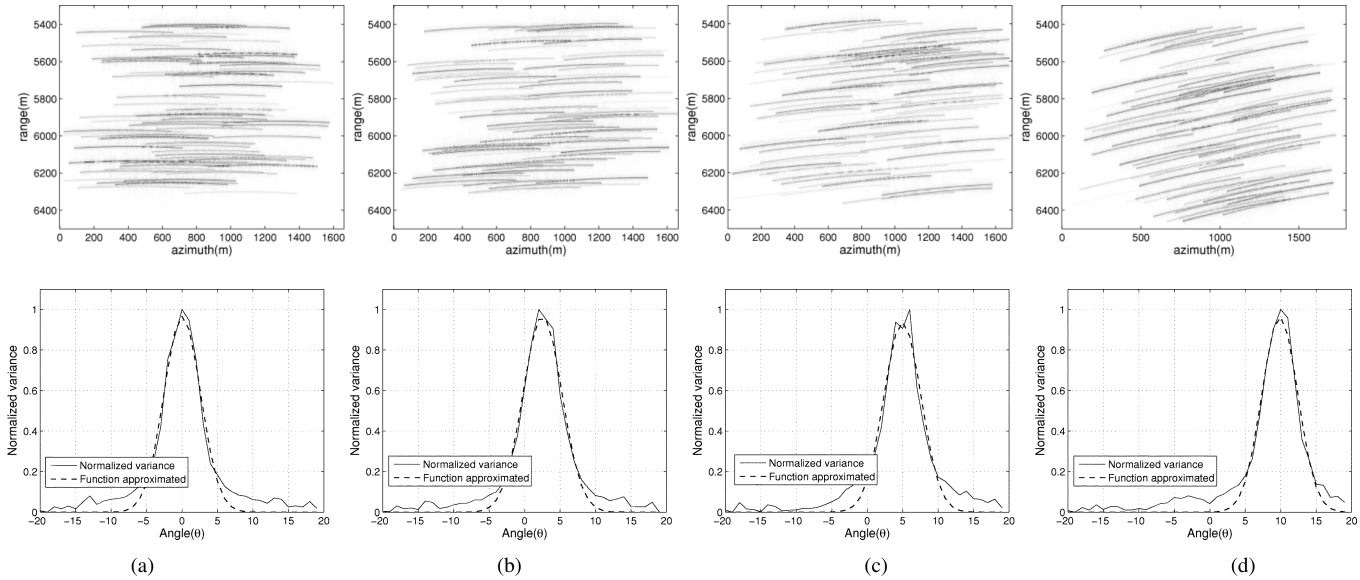

Fig. 5. Simulation results of the cases of multiple scatterers. The figures at the top show the range-compressed data, and the figures at the bottom show the estimated results using GDE. (a) Simulation dataset 1, $\theta_s = 0°$. (b) Simulation dataset 2, $\theta_s = 2.5°$. (c) Simulation dataset 3, $\theta_s = 5°$. (d) Simulation dataset 4, $\theta_s = 10.0°$.

TABLE I
SIMULATION RESULTS OF GDE AND CONVENTIONAL ALGORITHMS

θ_s(deg)	f_{DC}(Hz)	$\hat{f}_{DC}$(Hz)			
		GDE[1]	GDE[2]	CDE	ΔE
0.0	0	5.6	4.2	0.0	0.0
2.5	290.8	301.0	293.2	290.7	290.0
5.0	581.1	591.8	589.4	-417.6	-417.9
10.0	1157.7	1139.8	1142.6	155.9	159.2

GDE parameters are $R = 20$, $D = 2$, $\Delta\theta = 1°$.
[1] The Radon transform used RT algorithm 1.
[2] The Radon transform used RT algorithm 2.

B. Cases of the Multiple Point Scatterers

Second, the simulations of the case of multiple scatterers were performed, and the estimated results of GDE, CDE, and ΔE were compared. SDE could not be used in this simulations, because the simulated raw data are not circular symmetric Gaussian process, which is the basic requirement for SDE. The positions and the RCS's of the scatterers are randomly generated with uniform distribution. The simulation parameters are: 1) the number of scatterers $N_s = 100$, PRF $= 1000$ Hz, $f_s = 150$ MHz; 2) chirp bandwidth $f_{BW} = 100$ MHz; 3) the platform height $h = 2000$ m; 4) the ground range to the terrain $r_g = 5000$ m; and 5) $\beta_h = 6°$, $\theta_s = 0°$, 2.5°, 5.0°, 10.0°.

The simulation results are shown in Fig. 5 and Table I. The figures at the top in Fig. 5 show the range-compressed data of simulated raw data, and the figures at the bottom in Fig. 5 show the estimated results using GDE. As mentioned in Section III-B, two versions of the Radon transform were implemented, and the estimated results of these two implementations is compared in Table I. The accuracy of GDE did not show significant dependency on which of these two implementations of the Radon transform were used, as seen in Table I.

As no partially exposed target is in the simulated data, CDE and ΔE show exact results in the cases of $\theta_s = 0.0°$ and $\theta_s = 2.5°$. But, in the cases of $\theta_s = 5.0°$ and $\theta_s = 10.0°$, only GDE shows correct estimations. $f_{\rm DC}$ can be expressed as $f_{\rm DC} = M_{\rm amb} \cdot {\rm PRF} + f_a$, where $M_{\rm amb}$ is the ambiguity number and f_a is the ambiguous part of the Doppler centroid. f_a's estimated by CDE and ΔE are accurate in all cases, while $M_{\rm amb} = 0$ all the time for these algorithms. The estimated results by GDE do not show ambiguity and are accurate enough to be used in SAR processing. As seen in Table I, the accuracy of GDE is within 5% of the azimuth bandwidth. In general, the accuracy of the Doppler centroid must be within 5% to 10% of the azimuth bandwidth [3].

The computational load of GDE is scalable by adjusting the down-sampling factor D and the angular step size $\Delta\theta$. To examine the effect of D and $\Delta\theta$ on the estimation performance and the computation time, the simulation with different values of D and $\Delta\theta$ were performed, and the results are shown in Table II. In this simulation, the performance of GDE was satisfactory for $D = 1, 2$, but if D is larger than 2, the performance of GDE was degraded. If the angular step size $\Delta\theta$ is less than $\beta_h/3$, the accuracy of estimation was not affected by the value of $\Delta\theta$, as seen in Table II. As a reference, the computation times of CDE and ΔE were 0.7 and 6.5 s, respectively, for simulation datasets 2 and 3. To increase the accuracy of estimation, the combination of GDE and other conventional algorithms can be considered. If M is determined by GDE ($D = 4$, $\Delta\theta = 2.0$) and f_a is determined by CDE, the total computation time for simulation dataset 2 will be 1.3 s. If the $\hat{f}_{\rm DC}$'s shown in Table I estimated by CDE are corrected using the results of GDE, the corrected $\hat{f}_{\rm DC}$'s are 0.0, 290.7, 582.4, and 1155.9 Hz. These values of $\hat{f}_{\rm DC}$ are very accurate.

C. Effect of SNR On the Performance of GDE

At this point, the effects of SNR on the performance of GDE can be considered. As GDE estimates the average inclination angle of the range-compressed signal, the most important factor for the success of GDE is the existence of prominent targets. The number of prominent targets required is not so

TABLE II
EFFECTS OF DOWN-SAMPLING FACTOR (D) AND THE ANGULAR STEP SIZE ($\Delta\theta$) ON THE COMPUTATION TIME AND THE RESULT OF ESTIMATION

D [1]	f_{DC} [3]	$\hat{f}_{DC}$	T(sec)	f_{DC} [4]	$\hat{f}_{DC}$	T(sec)
1	290.8	298.3	3.6	581.1	592.1	3.7
2		293.2	1.3		589.4	1.3
4		243.4	0.6		585.2	0.6
8		197.2	0.3		582.8	0.3
$\Delta\theta(°)$ [2]		$\hat{f}_{DC}$	T(sec)		$\hat{f}_{DC}$	T(sec)
0.25		287.5	3.1		580.1	3.3
0.5		288.5	1.8		581.4	2.0
1.0		293.2	1.3		589.4	1.3
2.0		294.8	1.0		605.2	1.1

The Radon transform used RT algorithm 2.
[1] Simulations were performed with $\Delta\theta = 1.0°$
[2] Simulations were performed with D=2
[3] Simulation data set 2 was used.
[4] Simulation data set 3 was used.

many. This means that the scene contrast has no direct relation with the performance of GDE. To show this, we performed simulations using the simulation dataset of Fig. 5(d). We added complex Gaussian noise to range-compressed data and estimated the Doppler centroid using GDE. Here, SNR is defined as the ratio between the power of the most prominent target and noise power. The results are shown in Figs. 6 and 7. As SNR is getting smaller, unwanted spikes appear in variance curve (solid lines) in Fig. 6. It can be seen in Fig. 7 that the performance of GDE is robust against SNR if SNR of higher than about 0 dB is provided. But, if GDE is applied to real SAR data, an SNR of 3 dB is considered as the minimum.

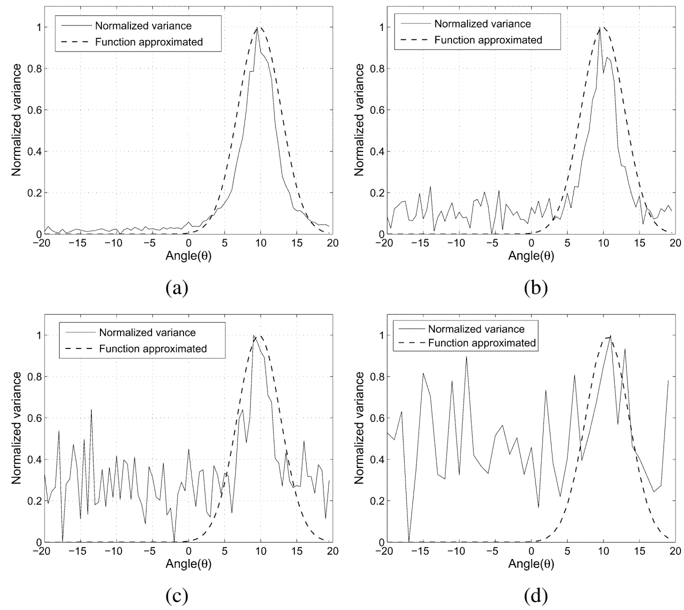

Fig. 6. Estimated results in several cases of SNR. If SNR is lower than 0 dB, the estimation results are not reliable. (a) SNR $= 10.0$ dB. (b) SNR $= 3.0$ dB. (c) SNR $= 0.0$ dB. (d) SNR $= -3.0$ dB.

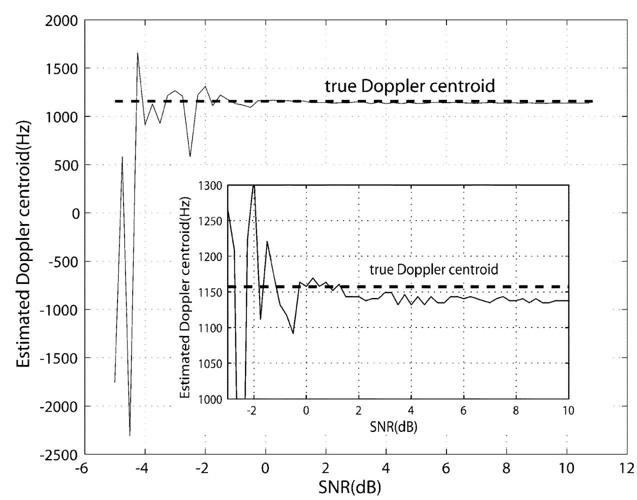

Fig. 7. Plot of estimated Doppler centroid versus SNR. Enlarged plot around the Doppler centroid is shown in the inset.

V. EXPERIMENTS

Four sets of airborne SAR data were used to evaluate the performance of GDE from two different SAR systems, denoted by characters of A and B. The basic SAR parameters are as follows:

- A1–A3: $f_c = 8.6$ GHz, $f_s = 113$ MHz, $f_{BW} = 100$ MHz, PRF $= 1923$ Hz, $V_{st} = 100$ m/s, $h = 4.3$ km;
- B1: $f_c = 9.15$ GHz, $f_s = 150$ MHz, $f_{BW} = 100$ MHz, PRF $= 2000$ Hz, $V_{st} = 103$ m/s, $h = 3.0$ km.

Table III shows the descriptions of the SAR data, and Fig. 8 shows the range-compressed images, and the variance $\hat{v}(j)$ along with the resultant function approximation for the four datasets. The estimated Doppler centroids of the conventional algorithms (ΔE, CDE, SDE) and GDE are compared in Table IV.

Because the contrast of dataset A1 is extremely low and no prominent targets exist in it, all the conventional algorithms show good performance. As seen in Fig. 8(a) and Table IV, the estimated result of GDE for dataset A1 is inaccurate when compared with conventional algorithms. But, assuming the true Doppler centroid to be 930 Hz, the error is less than 3%, which is acceptable for SAR processing. Although the contrast of dataset A2 is high, conventional algorithms show good results because the problem of partial coverage of strong targets is not severe in dataset A2. Note the results of dataset A3. The results of ΔE, CDE, and SDE show positive values, but the actual value must be negative, as can be seen from the range-compressed image of Fig. 8(c). This is due to the ambiguity problem that occurred

TABLE III
DESCRIPTION OF DATASETS

Data set	Description	No. of Pulses
A1	Mountain. No strong targets. Extremely low contrast	32768
A2	A port city with many man-made targets such as buildings, banks, and container boxes. High contrast.	65536
A3	Same port city as data set 2, different area. High contrast.	25000
B1	Rice fields and some man-made targets. Low contrast.	32768

when $f_{\mathrm{DC}} > |\mathrm{PRF}/2|$. GDE does not have this problem and shows a negative Doppler centroid as expected. An unwanted peak in variance curve in Fig. 8(c) appeared around $-4°$ due to partially exposed strong targets (in this case, ships). The effect of the unwanted peak to the estimated result was minimal, as seen from the bottom figure of Fig. 8(c). Scene of dataset B1

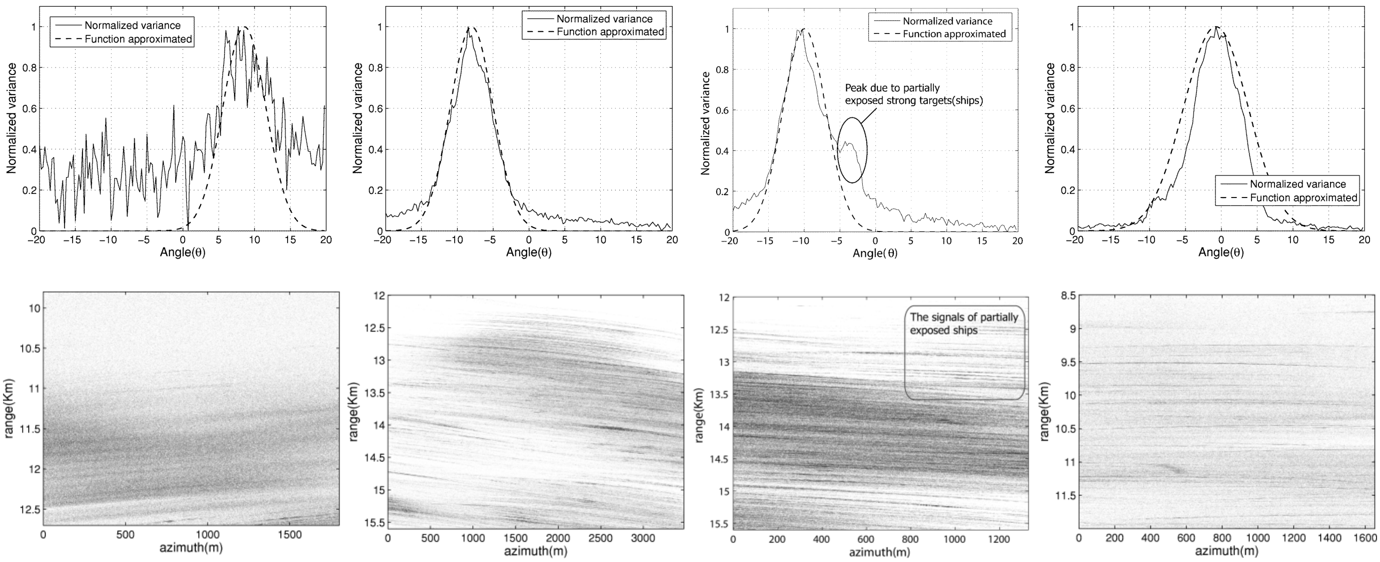

(a) (b) (c) (d)

Fig. 8. Range-compressed images at the top and the resultant function approximation (dashed lines) at the bottom. (a) Dataset A1. Due to no prominent targets in the scene, $\hat{f}_{\mathrm{DC}} = 877.1$ Hz of GDE is somewhat inaccurate when compared with conventional algorithms. (b) Dataset A2. As seen from the range-compressed image, the image is highly squinted about $-8.2°$. $\hat{f}_{\mathrm{DC}} = -820.7$ Hz seems to be reliable. (c) Dataset A3. Due to partially exposed strong targets (ships), unwanted peak is shown at $-4°$ in the bottom figure. Nevertheless the estimated result is acceptable. (d) Dataset B1. Scene is typical rice fields. As $\hat{\theta}_s = -0.6°$, no ambiguity problem occurs for all algorithms.

TABLE IV
ESTIMATED DOPPLER CENTROID VALUES USING GDE AND CONVENTIONAL ALGORITHMS (UNIT IS IN HERTZ)

Data set	GDE	ΔE	CDE	SDE
A1	877.1	929.5	933.1	938.0
A2	-820.7	-855.2	-810.9	-827.0
A3	-1066.5	890.9	915.1	948.9
B1	-64.5	-54.7	-48.6	-42.0

[A1-A3] GDE parameters are : R=26, D=2, $\Delta\theta$=0.25°, RT algorithm 2.
[B1] GDE parameters are : R=20, D=2, $\Delta\theta$=0.25°, RT algorithm 2.

is typical rice field with some man-made targets. Although the scene contrast is low, GDE estimated the Doppler centroid successfully as some prominent targets exist in that scene. The estimated results of all conventional algorithms are satisfactory.

As mentioned previously, SAR processing using inaccurate Doppler centroid results in geometric distortion. However, if the ambiguity number is estimated incorrectly, azimuth compression will totally fail as seen from Fig. 9. (However, in cases of spaceborne SAR, as f_{DC} can be as large as ±30 PRF [7], azimuth compression may not fail if ambiguity error is not severe.) Fig. 9(a) shows the SAR image using the correct Doppler centroid estimated by GDE, and Fig. 9(b) shows the SAR image using the incorrect Doppler centroid information estimated by conventional algorithms.

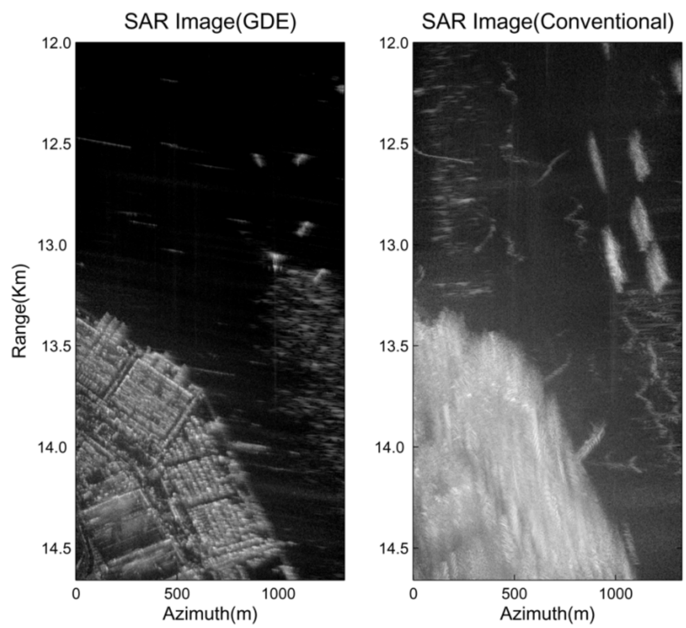

(a) (b)

Fig. 9. SAR images of dataset A3 applied only to coarse motion compensation. Image size is 2.6 km × 1.3 km. (a) SAR image processed using Doppler information from GDE. (b) SAR image processed using Doppler information from conventional algorithms.

VI. CONCLUSION

In this paper, we proposed an ambiguity-free Doppler centroid estimation technique using the Radon transform, called GDE. GDE utilizes the range walk induced by a squinted antenna beam or the yawing of the aircraft. It requires no Fourier transform and is computationally very efficient. To show the performance of GDE, we performed simulations and experiments using four sets of airborne SAR data with several squint angles. Through the simulations, the accuracy and the efficiency of GDE was verified. In experiments, GDE and all conventioal algorithms estimated the Doppler centroids of low-contrast datasets successfully. For highly squinted high-contrast datasets, only GDE successfully estimated f_{DC} without ambiguity, while the conventional algorithms failed to estimate the correct Doppler centroid.

REFERENCES

[1] S. N. Madsen, “Estimating the Doppler centroid of SAR data,” *IEEE Trans. Aerosp. Electron. Syst.*, vol. 25, no. 2, pp. 134–140, Mar. 1989.

[2] M. Y. Jin, “Optimal Doppler centroid estimation for SAR data from a quasihomogeneous source,” *IEEE Trans. Geosci. Remote Sens.*, vol. GE-24, no. 2, pp. 1022–1025, Mar. 1986.

[3] F. Wong and I. G. Cumming, “A combined SAR Doppler centroid estimation scheme based upon signal phase,” *IEEE Trans. Geosci. Remote Sens.*, vol. 34, no. 3, pp. 696–707, May 1996.

[4] R. Bamler, “Doppler frequency estimation and the Cramer-Rao bound,” *IEEE Trans. Geosci. Remote Sens.*, vol. 25, no. 3, pp. 385–390, May 1991.

[5] W. Yu and Z. Zhu, “Comparison of Doppler centroid estimation methods in SAR,” in *Proc. IEEE 1997 Nat. Conf.*, vol. 2, Jul. 1997, pp. 1015–1018.

[6] I. G. Cumming, P. F. Kavanagh, and M. R. Ito, “Resolving the Doppler ambiguity for spaceborne synthetic aperture radar,” in *Proc. IGARSS*, Sep. 1986, pp. 1639–1643.

[7] R. Bamler and H. Runge, “PRF-ambiguity resolving by wavelength diversity,” *IEEE Trans. Geosci. Remote Sens.*, vol. 29, no. 6, pp. 997–1003, Nov. 1991.

[8] J. Holzner and R. Bamler, “Burst-mode and scanSAR interferometry,” *IEEE Trans. Geosci. Remote Sens.*, vol. 40, no. 9, pp. 1917–1934, Sep. 2002.

[9] H. Simon, *Neural Networks*. Upper Saddle River, NJ: Prentice-Hall, 1999.

[10] M. L. Brady, “A fast discrete approximation algorithm for the radon transform,” *SIAM J. Comput.*, vol. 27, no. 1, pp. 107–119, Feb. 1998.

Young-Kyun Kong was born in Hwasoon, Korea, in 1975. He received the B.S. and M.S. degrees in electronic and electrical engineering from Pohang University of Science and Technology (POSTECH), Pohang, Korea, in 1998 and 2000, respectively. He is currently pursuing the Ph.D. degree at POSTECH.

Since 1998, he has worked on and developed an automobile-based SAR system (AutoSAR) and related control and signal processing software. His current research interests are airborne SAR signal processing. He joined the KOMSAR (KOrea Miniature SAR) Project for signal processing in 2003, and developed an airborne SAR signal processor for two SAR systems.

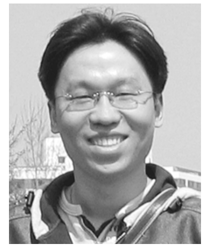

Byung-Lae Cho was born in Yeongcheon, Korea, in 1976. He received the B.S. degree in electronic and electrical engineering from Kyungpook National University, Daegu, Korea, and the M.S. degree from Pohang University of Science and Technology (POSTECH), Pohang, Korea, in 1999 and 2001, respectively. He is currently pursuing the Ph.D. degree in electronic and electrical engineering at POSTECH.

His research interests include SAR, interferometric SAR, and RCS measurement.

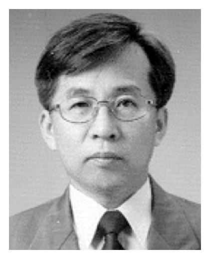

Young-Soo Kim (S’79–M’84) received the B.S. degree in electronic engineering from Seoul National University, Seoul, Korea, and the M.S. and Ph.D. degrees in electrical engineering from the University of Kansas, Lawrence, in 1974, 1980, and 1984, respectively.

From 1984 to 1987, he was with the Department of Electrical Engineering, Florida Atlantic University, Boca Raton, as an Assistant Professor. Since 1987, he has been with the Department of Electronics and Electrical Engineering, Pohang University of Science and Technology, Pohang, Korea as a Professor. From 1988 to 1994, he was with a multidisciplinary team of scientists and engineers for the successful design and construction of a third-generation synchrotron light source in Korea. From 1995 to 2003, he was in charge of the Remote Sensing Laboratory, Microwave Applications Research Center, funded by the Ministry of National Defence, Korea. His current research interests include microwave system design, radar remote sensing, EMI/EMC, RFID, and the spectrum engineering.